



Realization of high mass loading $\text{LiNi}_{0.5}\text{Mn}_{1.5}\text{O}_4$ Li-ion cathodes using water-soluble carrageenan as binder

Markus Binder^{a,b}, Eva Keller^c, Dominic Bresser^{a,b,*}

^a Helmholtz Institute Ulm (HIU), Helmholtzstrasse 11, 89081, Ulm, Germany

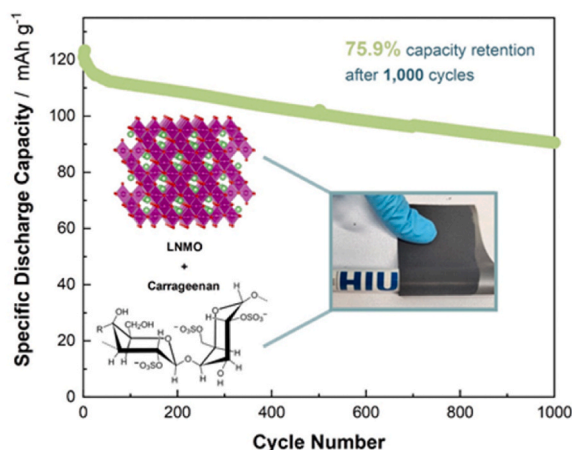
^b Karlsruhe Institute of Technology (KIT), P.O. Box 3640, 76021, Karlsruhe, Germany

^c Zentrum für Sonnenenergie- und Wasserstoff-Forschung Baden-Württemberg (ZSW), Helmholtzstrasse 8, 89081, Ulm, Germany

HIGHLIGHTS

- Fully aqueous processed graphite|| $\text{LiNi}_{0.5}\text{Mn}_{1.5}\text{O}_4$ lithium-ion cells.
- Realization of $\text{LiNi}_{0.5}\text{Mn}_{1.5}\text{O}_4$ electrodes with an areal capacity of 2.5 mAh cm^{-2} .
- First cycle Coulombic efficiency above 90%.
- Capacity retention of >75% after 1000 cycles.

GRAPHICAL ABSTRACT



ARTICLE INFO

Keywords:

Aqueous processing
Biopolymer
Cathode
 $\text{LiNi}_{0.5}\text{Mn}_{1.5}\text{O}_4$
Lithium-ion battery

ABSTRACT

Cobalt-free $\text{LiNi}_{0.5}\text{Mn}_{1.5}\text{O}_4$ (LNMO) is considered a very promising cathode material candidate for more sustainable lithium-ion batteries, especially when processed into electrodes using water-soluble, fluorine-free binding agents. However, the realization of high-performance electrodes with commercially relevant active material mass loadings remained challenging so far, as such binders are commonly rather brittle and/or suffer from an insufficient electrochemical stability towards oxidation. Herein, we report the use of (citric acid cross-linked) carrageenan as alternative binder for LNMO cathodes, enabling the realization of electrodes with an active material mass loading as high as 20 mg cm^{-2} . These electrodes show suitable mechanical, physicochemical, and electrochemical properties and offer very good cycle life and rate capability in half-cells graphite||LNMO full-cells with a capacity retention of about 76% after 1000 cycles at 1C. A particular advantage of carrageenan is that it is already available at industrial scale, rendering its practical use rather straightforward.

* Corresponding author. Helmholtz Institute Ulm (HIU), Helmholtzstrasse 11, 89081, Ulm, Germany.

E-mail address: dominic.bresser@kit.edu (D. Bresser).

<https://doi.org/10.1016/j.jpowsour.2024.234487>

Received 17 January 2024; Received in revised form 21 March 2024; Accepted 31 March 2024

Available online 5 April 2024

0378-7753/© 2024 The Authors. Published by Elsevier B.V. This is an open access article under the CC BY license (<http://creativecommons.org/licenses/by/4.0/>).

1. Introduction

Cobalt-free $\text{LiNi}_{0.5}\text{Mn}_{1.5}\text{O}_4$ (LNMO) is a very promising cathode material candidate for more sustainable lithium-ion batteries (LIBs) owing to its competitive energy density and high rate capability in combination with the low nickel content [1–4]. Nonetheless, the high de-/lithiation potential of about 4.7 V vs. Li^+/Li , which renders it so attractive in terms of energy and power density, poses also a great challenge with regard to the identification and development of suitable electrolytes that are sufficiently stable at such high potentials [5,6], especially in combination with a graphite-based anode [7–9]. Given the great promise, however, it has been studied for many years now, revealing important insights concerning the impact of the Mn^{3+} content [10], lattice doping [11–13], particle size/surface sites [14–17], and electrolyte composition [18–22] on the overall electrochemical performance. This great progress has helped to bring LNMO step by step closer to commercialization [4,23].

With regard to the potential advantages concerning sustainability and cost, it would be particularly beneficial to simultaneously replace the commonly used polyvinylidene fluoride (PVdF) by fluorine-free, water-soluble polymers as binder and, hence, also harmful *N*-methyl-2-pyrrolidone (NMP) by water as the electrode fabrication solvent. In fact, the replacement of NMP by water would allow for a significant cost reduction, since the evaporation and regeneration of NMP, as well as the generally required humidity control during electrode fabrication in such case, demands a lot of energy [1,24–26]. Moreover, fluorine-free binders are commonly less costly than the highly fluorinated PVdF, which further adds to the potential cost reduction and lower environmental footprint [27,28], while also the recycling of the resulting LIBs at their end of life would be significantly easier [25,26]. Several bio-derived polymers have been considered as fluorine-free binders in the past for LNMO cathodes, including, for instance, carboxymethyl cellulose (CMC) [29,30], guar gum (GG) [31–33], chitosan (CHI) [34,35], and alginate (ALG) [36,37]. All these studies, however, reported lab-scale electrodes with active material mass loadings (well) below 10 mg cm^{-2} – presumably, also because of the rather poor mechanical properties of the resulting electrodes when significantly exceeding this value, despite substantial progress when crosslinking the polymer with citric acid (CA) [38,39]. An alternative bio-derived polymer that has attracted only very little attention so far in this field – and has never been reported for LNMO cathodes yet to the best of our knowledge – is carrageenan (CAR) [40–42]. CAR can be obtained from algae and there are different isomers and phases of CAR known, depending on the chemical structure and the amount of sulfate functional groups per polymer unit [43]. A possible reason for the rather limited number of studies on this alternative binder might be the high viscosity of most CAR phases and isomers in aqueous solution [40,41], although this can be addressed by carefully selecting a suitable phase and counter ion [44,45].

Herein, a commercially available CAR is investigated as alternative water-soluble and fluorine-free binder for LNMO-based cathodes. It is demonstrated that CAR – after crosslinking with CA – outperforms other aqueous binders and provides comparable performance metrics as PVdF. Moreover, it is shown that the use of crosslinked CAR allows for the realization of flexible LNMO-cathodes with a commercially relevant active material mass loading of more than 20 mg cm^{-2} , which translates into an areal capacity of about 3 mAh cm^{-2} , representing a major step towards the scale-up of water-processed, fluorine-free lithium-ion cathodes.

2. Experimental section

2.1. Electrode preparation

The LNMO electrodes comprised varying compositions of 88–92 wt% LNMO (Haldor Topsoe), 2–8 wt% conductive carbon (Imerys, CNERGY Super C45), and 2–4 wt% binder. The different binders, i.e., carrageenan

(CAR, CP Kelco Genuvisco® CG-129), carboxymethyl cellulose (CMC, Waloce CRT 2000 GA 07, degree of substitution 0.7, Dow Wolff Cellulosics), guar gum (Lamberti), and polyvinylidene difluoride (PVdF, Solvay 6020) were first dissolved either in deionized water or, in the case of PVdF, in NMP (anhydrous, 99.5% Sigma-Aldrich). In some cases, as indicated in the text and figures, citric acid (CA, 99%, Sigma-Aldrich) was added to the water-soluble binders in a 9:1 ratio, serving as cross-linking agent for the water-soluble binders used herein, as reported earlier by Kuenzel et al. [30,33]. After having added the conductive carbon and the LNMO active material, 1 wt% (with respect to the active material) phosphoric acid (PA, >99%, Bernd Kraft) was added as well, and the mixture was homogenized using a planetary mixer (ARE-250, Thinky). The addition of PA – in addition to the use of CA – helps to decrease the pH of the slurry below 9 (a regime where the aluminum foil is stable towards corrosion). Moreover, it results in the formation of a thin metal phosphate surface layer on the LNMO particles, which has been shown to be beneficial for the interfacial stability with the electrolyte and, thus, the overall performance of the resulting electrodes [30,46–48]. The resulting slurry was cast on carbon-coated aluminum foil (battery grade) with a laboratory-scale doctor blade (wet film thickness: $120 \mu\text{m}$). The wet electrodes were pre-dried for 15 min at $80 \text{ }^\circ\text{C}$ and further dried overnight at room temperature in a dry room with a dew point of less than $-70 \text{ }^\circ\text{C}$. Subsequently, disc-shaped electrodes with a diameter of 12 mm were cut from the electrode tape and pressed at 5 t for 15 s (Atlas manual hydraulic press, Specac) prior to the final drying under vacuum ($<10^{-3} \text{ mbar}$) at $120 \text{ }^\circ\text{C}$ for 14 h. The eventual active material mass loading was either about 6, 13, or 20 mg cm^{-2} . All electrodes showed a final porosity between 35 and 43% (see Table S1 and Table S2 as well as the corresponding discussion in the Supporting Information for more details). For the preparation of the graphite-based anodes, 94 wt% of the graphite active material (TIMREX SLP30, Timcal), 2 wt% CMC, 2 wt% styrene-butadiene rubber (SBR, TRD102A, JSR Micro), and 2 wt% of conductive carbon (CNERGY Super C45, Imerys) were mixed in deionized water once the CMC had been fully dissolved. The dispersion was homogenized using the same planetary mixer as used for the LNMO electrodes, and eventually cast on battery-grade copper foil (Schlenk) using a laboratory-scale doctor blade. The active material mass loading was $8.0\text{--}8.2 \text{ mg cm}^{-2}$. The model electrodes for the determination of the electrochemical stability of the binder consisted of 95 wt% of conductive carbon (Imerys CNERGY Super C45) and 5 wt% of the given binder with a dry mass of $\sim 2 \text{ mg cm}^{-2}$. These electrodes were prepared in the same manner as the LNMO electrodes, i.e., mixed with a Thinky mixer and cast on a battery-grade carbon-coated aluminum foil.

2.2. Physicochemical characterization

Thermogravimetric analysis (TGA) was conducted using a Netzsch STA 409 PC, increasing the temperature from room temperature up to $500 \text{ }^\circ\text{C}$ at a heating rate of $10 \text{ }^\circ\text{C min}^{-1}$ under nitrogen atmosphere. The phase-pure CAR references, i.e., lambda-CAR and iota-CAR were acquired from Sigma-Aldrich. Fourier-transform infrared (FTIR) spectroscopy was performed using a PerkinElmer Spectrum Two Spectrometer in the range from 500 to 4000 cm^{-1} , averaging the data obtained over five spectra with a resolution of 0.5 cm^{-1} . Scanning electron microscopy (SEM) was conducted using a Zeiss Crossbeam XB340 field-emission electron microscope equipped with energy-dispersive X-ray (EDX) spectroscopy detector (Oxford Instruments X-Max Xtreme, 100 mm^2 , 1–5 kV). For the SEM and EDX analysis, the acceleration voltage was set to 3 and 10 keV, respectively. Adhesion tests were performed according to TAPPI T541 with a ZwickiLine 2.5 kN (ZwickRoell). For these measurements, an electrode piece with an area of 6.45 cm^2 was fixed on the sample holder using adhesive tape (TESA tesafix 5696 extra strong). The compression stress was set to 2500 N with a dwell time of 30 s, followed by the adhesion tests with a pull-off velocity of 100 mm min^{-1} . A detailed description of the experimental

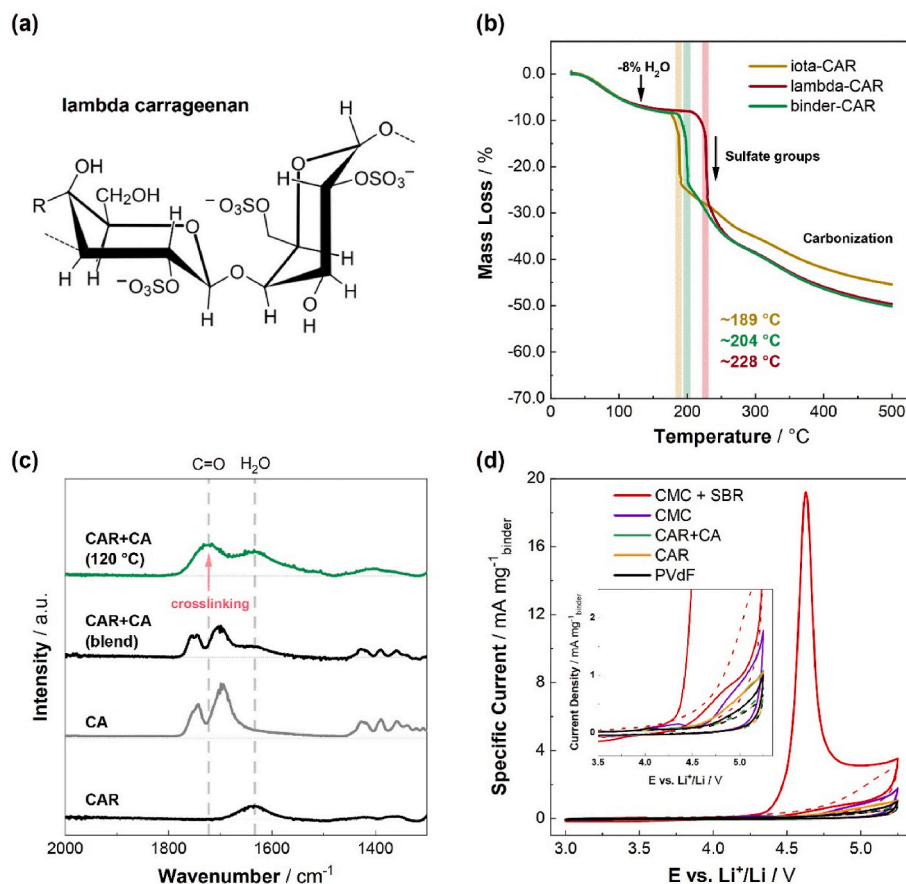


Fig. 1. (a) Chemical structure of lambda-CAR. (b) Thermogravimetric analysis of two phase-pure CAR samples (iota and lambda) and the commercial carrageenan used herein as binder ('binder-CAR'). (c) FTIR spectra of carrageenan (CAR, i.e., 'binder-CAR'), citric acid (CA), a blend of CAR and CA, and the blend CAR + CA heated to 120 °C. (d) Electrochemical stability against oxidation measured for carbon-based model electrodes containing different binders between 3.0 and 5.25 V vs. Li^+/Li with a sweep rate of 0.25 mV s^{-1} . The dashed lines represent the 3rd cyclic sweep.

setup and the influence of different parameters has been reported by Haselrieder et al. [49]. Also the compression tests were performed with a ZwickiLine 2.5 kN, using a flat tip with diameter of 5 mm^2 , a pre-load of 0.2 N for the determination of h_0 , and a measurement speed of 0.5 mm min^{-1} . The maximum force applied was 200 N, translating into a pressure of 40 MPa. The contact angle measurements were performed with the drop shape analyzer DSA100 Large (Krüss Optronic) and a drop volume of 2.0–3.5 μL . After an equilibration time of 10 s the contact angle remained constant for several minutes before water evaporation set in, resulting in a decreasing drop volume and, hence, contact angle. Thus, the measurement time was fixed to 60 s after placing the droplet. The viscosity was determined at room temperature ($23 \pm 2 \text{ }^\circ\text{C}$), using an Anton Paar ViscoQC300 viscometer with an L4 spindle and a sample volume of 100 mL. For each measurement speed, the equilibration time was set to 2 min. Additionally, the viscosity was determined in the Anton Paar "TruMode", in which the device is operating at its optimum torque of 80%, resulting in a better comparability among the different samples.

2.3. Electrochemical characterization

The electrochemical characterization was conducted in three-electrode Swagelok® cells, employing either lithium metal foil (thickness 500 μm , battery grade, Honjo Metal) or graphite electrodes as counter electrodes. The reference electrodes always consisted of metallic lithium. The cell assembly was carried out in an argon-filled glove box (MB200B ECO, MBraun) with a H_2O and O_2 content of less than 0.1 ppm. Glass fiber sheets (Whatman GF/D) served as separator and were soaked with 130 μL of the electrolyte (1 M LiPF_6 in ethylene carbonate (EC)/

dimethyl carbonate (DMC), 1:1 w/w, UBE – LP30). Galvanostatic cycling was performed within a voltage range from 2.8 to 5.0 V for the $\text{Li}||\text{LNMO}$ cells and from 2.8 to 4.9 V for the graphite $||\text{LNMO}$ cells, including a constant voltage step at 4.9 V. All tests were carried out at $20 \pm 2 \text{ }^\circ\text{C}$ utilizing a Maccor Battery Tester 4300. A dis-/charge rate of 1C corresponds to a specific current of 147 mA g^{-1} . For the cyclic voltammetry measurements, a VMP multichannel potentiostat (BioLogic) was used. For the determination of the electrochemical stability of the different binders using the model electrodes, a sweep rate of 0.25 mV s^{-1} was applied within a potential range from 3.0 to 5.25 V vs. Li^+/Li . For the cyclic voltammetry tests on the LNMO electrodes containing PVdF, CMC + CA, and CAR + CA, the sweep rate was set to 0.1 mV s^{-1} in a potential range from 3.0 to 4.9 V vs. Li^+/Li .

For the determination of the pore ion resistance R_{ion} , symmetric LNMO $||\text{LNMO}$ cells were assembled employing two-electrode Swagelok®-type cells, a glass fiber separator and 130 μL of the electrolyte. After a 24 h rest step, electrochemical impedance spectroscopy (EIS) measurements were performed in potentiostatic mode in a frequency range from 100 kHz to 100 mHz, with 10 points for every decade, and a voltage amplitude of 10 mV.

3. Results and discussion

The chemical structure of CAR is shown in Fig. 1a (exemplarily for the lambda phase; see also the forthcoming discussion). For the initial characterization, we conducted TGA on the commercial CAR used herein and two phase-pure CAR materials, i.e., iota-CAR (bearing two sulfate groups per two galactose units) and lambda-CAR (bearing three

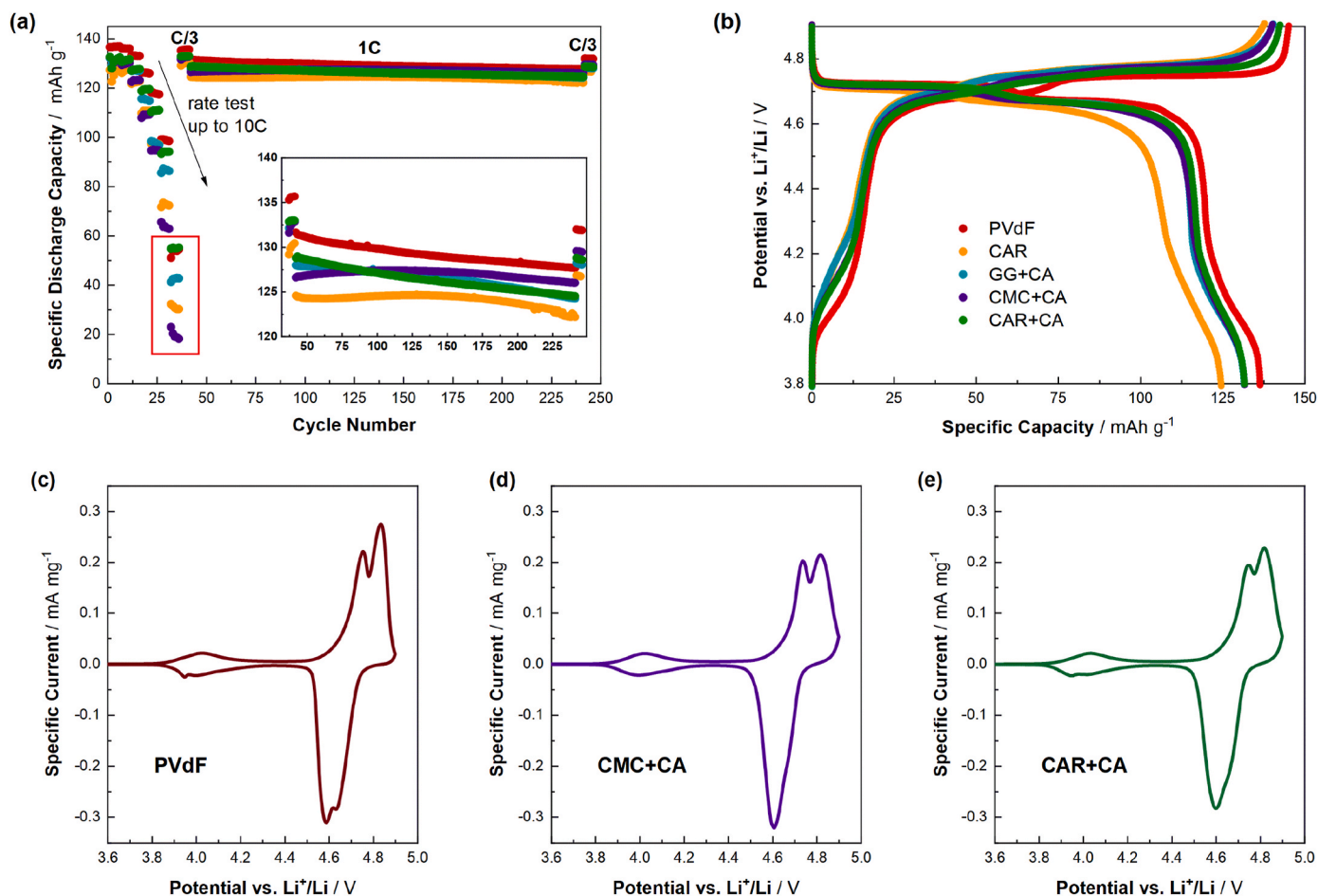


Fig. 2. (a) Galvanostatic cycling of Li||LNMO cells with different binders and a composition of 90:7:3 (active material: conductive carbon: binder) at varying C rates (C/3, C/2, 1C, 2C, 3C, 5C, 10C, and C/3) followed by 200 Cycles at 1C, and eventually five cycles at C/3; the inset shows a magnification of the cycles conducted at 1C (cut-off potentials: 2.8 and 5.0 V). (b) The corresponding dis-/charge profiles of the 1st cycle. (c–e) Cyclic voltammetry results obtained for LNMO electrodes containing (c) PVdF, (d) CMC + CA, and (e) CAR + CA as binder, employing a sweep rate of 0.1 mV s^{-1} (here, the 6th cyclic sweep is shown, following five formation cycles at the same sweep rate to account for the initial capacity increase observed upon galvanostatic cycling in the case of the water-soluble binders).

sulfate groups per two galactose units). While the phase-pure materials were purchased as sodium salts, the commercial CAR contains Na^+ and K^+ as counter ions. The results of the TGA are shown in Fig. 1b. All three samples contained around 8 wt% of water, which was lost in the temperature range up to $150 \text{ }^\circ\text{C}$. The subsequent mass loss between 185 and $235 \text{ }^\circ\text{C}$ can be attributed to the loss of the sulfate groups [41,50]. The herein used commercial CAR resembled initially iota-CAR during the steep mass loss in this temperature range, but subsequently merged with the TGA curve of lambda-CAR and, eventually, showed the same overall mass loss. This might indicate that the commercial CAR used herein also contains three sulfate groups, i.e., corresponds to the lambda phase. Nonetheless, the different TGA signature in combination with the varying onset temperature for the steep mass loss – with about $204 \text{ }^\circ\text{C}$ being a little closer to phase-pure iota-CAR ($189 \text{ }^\circ\text{C}$) than lambda-CAR ($228 \text{ }^\circ\text{C}$) – suggests that either the difference of the counter ions plays an important role as well, and/or that the three samples have a significantly different molecular mass, and/or that the CAR used herein is not a phase-pure material; the latter, in fact, is rather likely given the available scale and cost of the different materials. An in-depth “reverse-engineering” of the commercial CAR, however, has been beyond the scope of this study. Generally, the herein used CAR was thermally stable until about $200 \text{ }^\circ\text{C}$, which renders it suitable for the application as binder, since the electrode drying temperature is commonly well below $200 \text{ }^\circ\text{C}$, especially for water-based systems [51]. With regard to the beneficial effect of crosslinking such cellulose derivatives via CA by

esterification, as earlier shown for CMC [30] and GG [33], we comparatively investigated neat CAR and CA-crosslinked CAR (CAR + CA) in the following. The successful crosslinking was confirmed by FTIR spectroscopy (Fig. 1c). Just as reported for CMC [30] and GG [33], the simple blend of CAR and CA yields a simple combination of the FTIR spectra of CAR and CA, while the subsequent treatment at $120 \text{ }^\circ\text{C}$ (as used for drying the electrodes) resulted in a modification of the spectrum: the two distinct carbonyl bands of CA at around 1700 cm^{-1} merge into one single band, which can be assigned to the ester group resulting from the esterification-type crosslinking reaction [30,33]. To complete the initial characterization concerning the general suitability of (CA-crosslinked) CAR as binder for LNMO-based cathodes, we determined the electrochemical stability towards oxidation using electrodes comprising solely the binder and conductive carbon, and compared the results with neat CMC and CMC-SBR; the latter being commonly used for commercial graphite-based anodes [38,52]. The results are presented in Fig. 1d. CMC-SBR showed a very high specific current peak at about 4.5 V , indicating a severe oxidative decomposition process and rendering it non-suitable for application in LNMO-based cathodes. The comparison with neat CMC revealed that this oxidative decomposition reaction is related to the presence of SBR, in fact. While the current substantially decreased during cycling (the dashed line in the figure shows the 3rd cyclic sweep), it remained higher than for the other water-soluble binders, as also evident from the magnification of the high-voltage region in the inset in Fig. 1d. The magnification moreover shows that the

lowest current can be observed for PVdF, serving as reference with regard to currently used binders. However, CAR and CAR + CA show a very comparable current evolution, much lower than the CMC-based electrodes. Furthermore, the current stabilizes after 3 cycles to values below 1 mA mg^{-1} (referring to the mass of binder), which is essentially identical to the 3rd cycle of the PVdF-based model electrode. Given the limited electrochemical stability of the carbonate-based electrolyte used for these experiments, the very stable current evolution starting from the second cyclic sweep might be simply related to electrolyte oxidation at the electrode|electrolyte interface [53,54].

In fact, the difference between PVdF and CAR in the first cycle appears negligible, so that a significant binder decomposition can be excluded. Accordingly, CAR and CAR + CA appeared as potentially suitable binders for LNMO-based cathodes – not least given the very good results reported earlier for CMC [30,55]. In a next step, we compared CAR and CAR + CA as binder for LNMO-based electrodes with PVdF as well as CMC + CA and GG + CA via galvanostatic cycling of Li||LNMO cells at varying C rates (Fig. 2). For this initial comparison, an active material mass loading of about 6 mg cm^{-2} was used to avoid any detrimental impact of electrode cracking and other detrimental features when increasing the mass loading. Among the water-soluble binders, CAR + CA showed the highest reversible capacity, i.e., 133 mAh g^{-1} at C/3 (Fig. 2a), which was only ca. 2% less than the PVdF-based electrode. Moreover, the CAR + CA electrodes provided about 42% of its initial capacity at 10C, which was also very comparable with the PVdF-based electrodes – and outperforming the other electrodes such as CMC + CA, which provided only about 14% of its initial reversible capacity at 10C. During the 200 cycles at 1C (a magnification is shown as inset in Fig. 2a) the CAR + CA electrodes showed essentially the same linear capacity fade as the PVdF reference with a capacity loss of 3.3% compared to 2.8% for PVdF. The GG + CA and CAR electrodes showed a more stable capacity retention during the initial ~100 cycles, but a more pronounced fading afterwards. The CMC + CA electrodes showed a slight increase initially, before the capacity slightly decreased. Generally, the three electrodes containing the CA-crosslinked binders displayed a rather similar cycling stability, but the best rate capability was observed for CAR + CA, indicating superior de-/lithiation kinetics. This observation was in line with the comparison of the 1st cycle dis-/charge profiles (Fig. 2b), revealing the lowest polarization for CAR + CA compared to the other water-soluble binders, though being slightly higher than the PVdF reference, for which the two potential plateaus related to the redox activity of nickel are most pronounced. This trend is confirmed by the comparison of the corresponding cyclic voltammograms for the electrode containing PVdF, CMC + CA, and CAR + CA (Fig. 2c–e). In general, all three show the characteristic shape, including the $\text{Mn}^{3+}/\text{Mn}^{4+}$ couple at around 4.0 V and the two steps from Ni^{2+} to Ni^{3+} and further to Ni^{4+} at about 4.7 V [15,56]. Nonetheless, the electrodes containing PVdF reveal the most separated redox peaks for the two consecutive oxidation and, in particular, the reduction processes of nickel (Fig. 2c), while the latter are less easily distinguishable for CMC + CA (Fig. 2d) and CAR + CA (Fig. 2e), indicating a more sluggish electron transfer for the two water-soluble binders [57].

In sum, these findings do not only indicate a comparable or even better performance of CAR + CA compared to CMC + CA and GG + CA, but also underline once more the beneficial impact of the CA-induced crosslinking, yielding a higher reversible capacity and better rate capability than neat CAR. To characterize the effective ionic conductivity inside the porous electrode, the pore ion resistance R_{ion} as a potential indicator was determined for symmetric LNMO||LNMO cells containing PVdF, CMC + CA, and CAR + CA as binder (Fig. S1) [58,59]. The comparison revealed that PVdF and CMC + CA had an identical R_{ion} of ca. 4.3Ω , while it was slightly higher for CAR + CA with about 5.8Ω . This minor difference might point at a slightly different interaction between the binder and the LNMO particles, while the rate capability of CAR + CA was shown to be comparable to PVdF and superior to CMC + CA (see Fig. 2a).

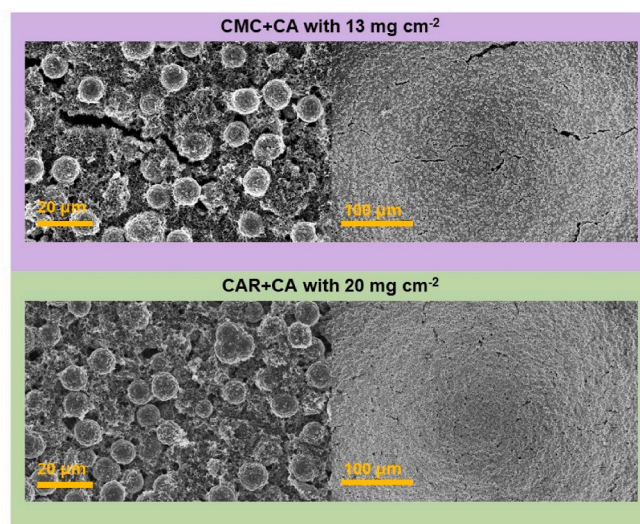


Fig. 3. SEM micrographs of LNMO electrodes with an active material mass loading of 13 mg cm^{-2} and CMC + CA as binder (top, purple background) and with an active material mass loading of 20 mg cm^{-2} and CAR + CA as binder (bottom, green background).

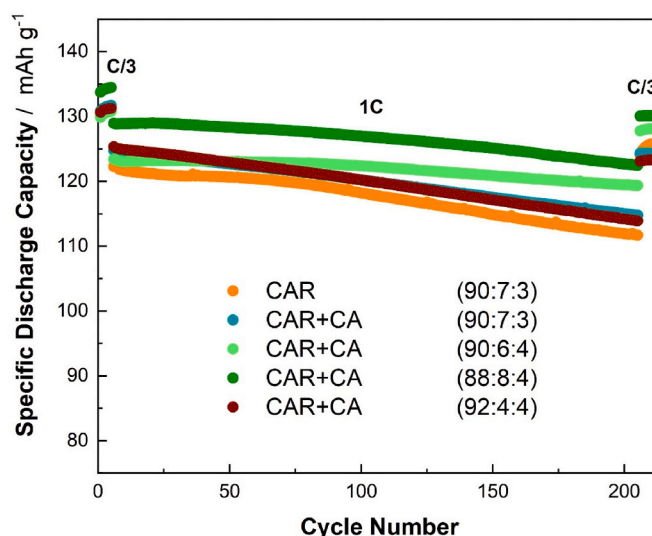


Fig. 4. Galvanostatic cycling of LNMO electrodes in half-cell configuration with varying electrode compositions using CAR or CAR + CA as binder and an active material mass loading of about 13 mg cm^{-2} (cut-off potentials: 2.8 and 5.0 V). The given electrode component ratios refer to the LNMO:carbon:CAR (+CA) ratio.

More importantly, in fact, the use of CAR allowed for the preparation of mechanically stable electrodes with substantially higher active material mass loadings without delamination from the current collector, cracking, or bending, indicating that there was less stress occurring during the drying process and resulting in a greater flexibility of the coating layer. In fact, a CMC + CA electrode with an active material mass loading of 13 mg cm^{-2} showed already several severe cracks in the coating layer (Fig. 3, top), which led to delamination issues during calendaring/pressing. Differently, no severe cracks were observed for CAR + CA, despite a much higher mass loading of about 20 mg cm^{-2} (Fig. 3, bottom). The minor cracks found even disappeared during calendaring/pressing (Fig. S2), rendering CAR + CA very suitable for yielding high mass loading electrodes. For a more quantitative comparison of the mechanical properties of the two different electrodes, a

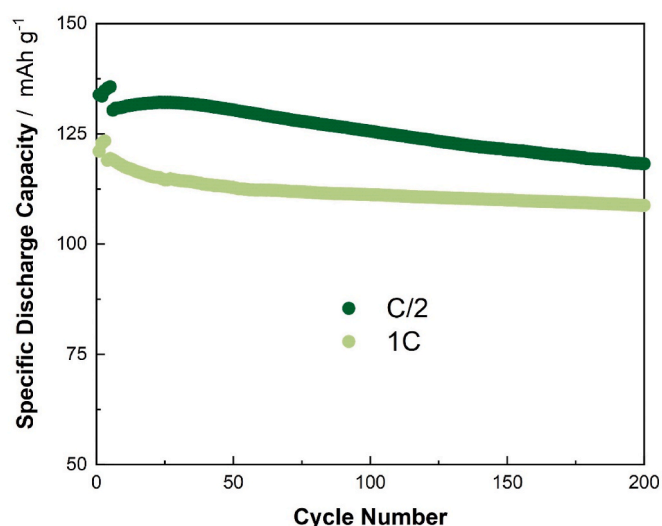


Fig. 5. Galvanostatic cycling of Li||LNMO cells with a high mass loading of about 20 mg cm^{-2} at a C rate of C/2 (dark red) and 1C (light red) after 5 formation cycles at C/3 (cut-off potentials: 2.8 and 5.0 V).

mandrel bending test was performed. For this, the mid-loading CMC + CA electrodes (13 mg cm^{-2}) and the high-loading CAR + CA electrodes (20 mg cm^{-2}) were bent over a polyvinyl chloride (PVC) rod with a decreasing diameter and investigated via optical microscopy under a 24-fold magnification (Fig. S3). According to the literature, a typical mandrel of a 21700 cylindrical cell has a diameter of 4 mm [60]. Consequently, our bending test approached a final bending diameter of 4 mm. In the case of the mid-loading CMC + CA electrodes, we observed severe cracks already at the largest diameter of 10 mm, which further increased when decreasing the bending diameter towards the eventual 4 mm. In contrast, the CAR + CA electrode sheets revealed an intact surface without cracks even for the smallest diameter. This experiment confirmed the potential use of the herein presented CAR + CA-based electrodes in commercial cylindrical cells.

In a subsequent step, we optimized the electrode composition for CAR + CA electrodes (in comparison with electrodes comprising neat CAR as binder) for an intermediate mass loading of 13 mg cm^{-2} (Fig. 4). In fact, the electrodes containing the neat CAR performed the worst, while the best cycling stability and highest reversible capacity were observed for an LNMO:carbon:CAR + CAR ratio of 88:8:4 with a reversible specific capacity of 135 mAh g^{-1} at C/3 and a capacity retention of 96.7% after 200 cycles at 1C. Apparently (in the given range), a higher binder and carbon content turned out advantageous. Nonetheless, the relatively high carbon content in this case led to rather brittle electrodes owing to the high surface area of the conductive carbon, causing a so-called “mud-cracking” phenomenon during solvent evaporation [61], which rendered a further increase in mass loading challenging.

For this reason, we chose the 92:4:4 ratio as a compromise between performance and processability for the further increase in mass loading up to 20 mg cm^{-2} . The galvanostatic cycling of such high mass loading electrodes in Li||LNMO cells at a dis-/charge rate of 1C and 0.5C is displayed in Fig. 5. The cells provided a reversible specific capacity of 131 mAh g^{-1} (0.5C) and 120 mAh g^{-1} (1C) with a very good capacity retention of about 91% after 200 cycles in both cases. It is noteworthy that we increased the initial rest time in this case from 12 h to 24 h, as the electrolyte wetting becomes an important factor at such high mass loadings, especially when considering the lab-scale cell assembly that involves the simple addition of the electrolyte on the separator. In fact, the initial increase in capacity upon cycling was greatly reduced for an initial rest step of 24 h compared to a rest step of only 12 h, as apparent from Fig. S4.

Motivated by this very good electrochemical performance, we characterized these high mass loading electrodes in more detail – to start with by an SEM and EDX analysis of the electrode surface and its cross-section (Fig. 6). Generally, the SEM micrographs showed crack-free electrodes with a good contact to the aluminum current collector. The accompanying EDX mapping revealed a homogeneous distribution of the active material, carbon and binder across the surface and the cross-section, i.e., in all three dimensions of the thick CAR + CA electrodes. Such homogeneity is an important pre-requisite to achieve a good electrochemical performance, especially for higher mass loadings, since

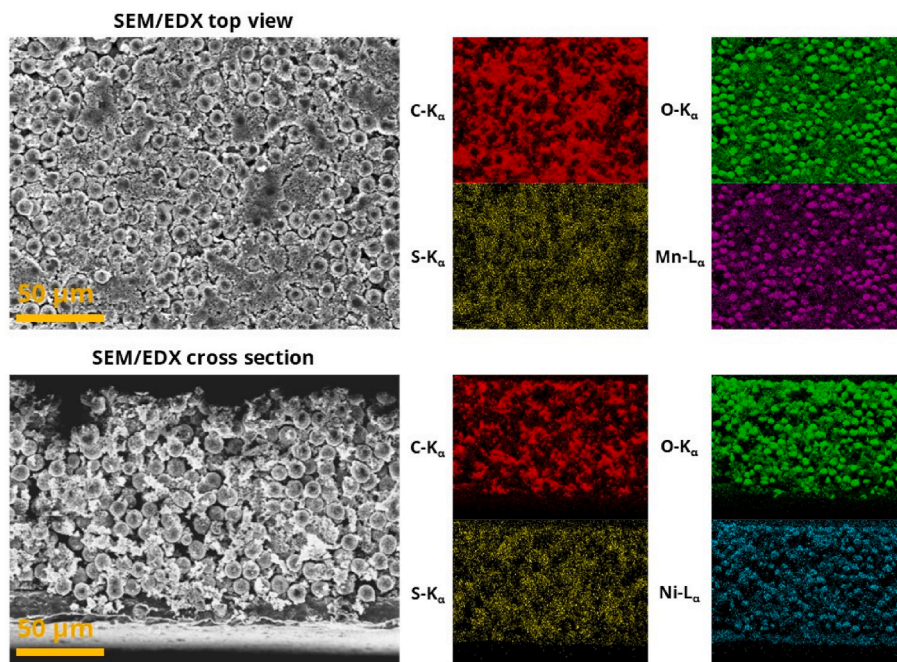


Fig. 6. SEM micrographs (top view and cross-section) and the corresponding EDX mappings for carbon (in red), oxygen (in green), sulfur (in yellow), and nickel (in turquoise) of CAR + CA-based LNMO electrodes with an active material mass loading of 20 mg cm^{-2} .

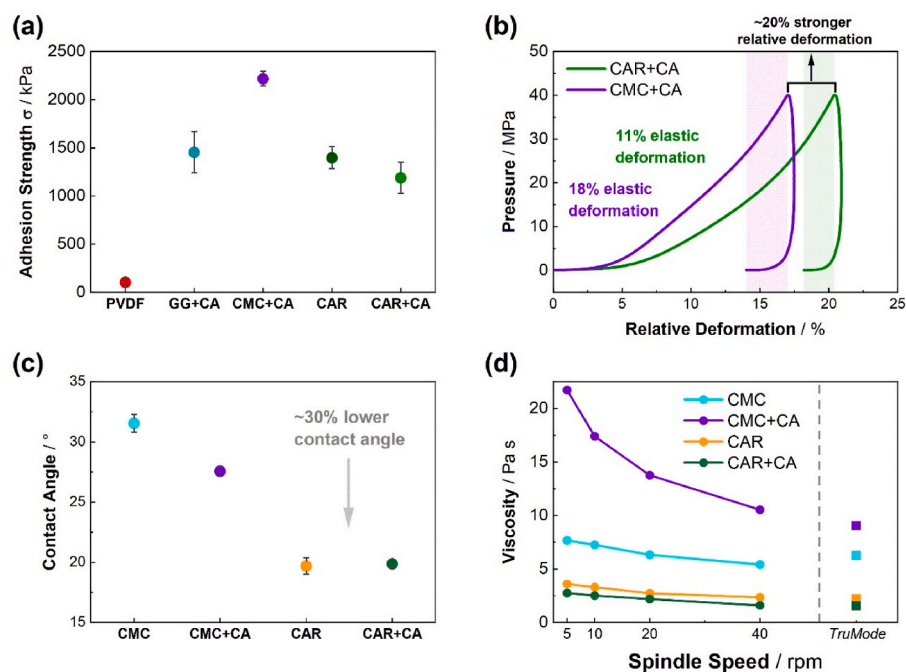


Fig. 7. (a) Determination of the adhesion strength of electrode coatings containing different binders with an active material mass loading of 6 mg cm^{-2} . (b) Relative deformation of electrode coatings containing CAR + CA and CMC + CA as binder with an active material mass loading of about 13 mg cm^{-2} (non-pressed). (c) Contact angle of the corresponding 3 wt% aqueous binder solutions on carbon-coated aluminum foil serving as current collector. (d) Viscosity of the 3 wt% aqueous binder solutions as a function of the spindle speed and in TruMode.

the risk of binder migration during electrode drying increases for increasing coating thicknesses.

While the major parameter influencing the binder migration is the drying temperature [62–64], also the choice of the binder plays an important role, depending on its tendency to migrate within the electrode. To evaluate the migration behavior, the adhesion of the electrode coating is frequently used as a quality measure, especially for new binder systems. Following our measurements, all water-soluble binders showed a substantially higher adhesion strength than PVdF (Fig. 7a), with the value for the latter being in good agreement with previously reported data [49]. Apparently, all binders are characterized by a sufficiently high adhesion, while the comparison of the electrochemical data underlines that a higher adhesion does not directly translate into better electrochemical performance [65]. Besides, the comparison of the adhesion strength does not allow for an explanation why CAR + CA is the only binder system out of these three that enables the successful preparation of high mass loading electrodes. One issue for GG, in fact, that is not reflected by these data, is the high viscosity of an aqueous GG solution, resulting in a relatively low potential solid content in the slurry. Accordingly, we focused on the comparison of CMC + CA and CAR + CA for the further characterization via compression tests. For such a tests, a maximum pressure of 40 MPa was applied to the non-pressed electrodes, and the deformation of the coating layer in comparison to the starting thickness h_0 was tracked (Fig. 7b). The results provide insights into the plastic and elastic deformation and, hence, the mechanical elasticity of the coating layer. The comparison of the two binder systems revealed that the CAR + CA electrodes showed a 20% stronger relative compression. This means that the CAR + CA electrodes require less force during calendaring to reach a certain density/thickness, which translates into less mechanical stress during the calendaring process. Moreover, the CAR + CA electrodes showed only about 11% elastic deformation compared to 18% for the CMC + CA electrode. The higher elasticity of the CMC + CA electrodes leads to a stronger springback effect after the calendaring process, thus, further increasing the stress in the coating layer and promoting the formation of defects [66,67]. In fact, the more pronounced plastic deformation recorded for

the CAR + CA electrodes might also explain why the very small cracks observed in the SEM micrographs of the CAR + CA electrodes vanished after calendaring the electrodes (Fig. S2), i.e., the rather plastic behavior results in a permanent rearrangement of the LNMO and carbon particles.

Another important measure for the realization of homogenous and crack-free coating layers is the surface tension of the processing solvent. It is known that the high surface tension of water, which is much higher than the one of NMP, can cause mud-cracking upon drying [61,68]. The contact angle is an easily measurable indication of the surface tension, and a comparison of the aqueous solutions of CMC, CMC + CA, CAR, and CAR + CA is presented in Fig. 7c – all measured on the carbon-coated aluminum foil used as current collector for the LNMO electrodes. These polysaccharides act as anionic surfactants in an aqueous solution and, thus, decrease the surface tension of water. Remarkably, the decrease in surface tension was about 30% greater for CAR(+CA) than for CMC(+CA), which might be attributed to the presence of the sulfate groups. As illustrated for water/isopropanol mixtures by Wood et al. [68], such a decrease in surface tension can mitigate the crack formation and thereby enable a higher critical coating thickness.

The advantageous properties of CAR(+CA) became apparent also from a comparison of the viscosity of the four solutions (Fig. 7d). While the addition of CA led to 44% higher viscosity in the case of CMC, it decreased by about 30% in the case of CAR on a generally much lower level. This result renders the CAR + CA solution favorable for electrode slurries with a high solid content and the electrode preparation via, e.g., doctor blade casting, comma bar or slot-die coating. The possibly higher solid content also translates into less water that needs to be evaporated eventually, thus, further reducing the stress in the electrode during drying – and requiring less energy for the drying process. It is important to note that the trends concerning the viscosity and the contact angle were not the same, i.e., the lower contact angle was not directly linked to the lower viscosity, but appears to be a material property of CAR as such.

In sum, the comparative evaluation of the different aqueous binders revealed that the use of CAR + CA results in less stress during the electrode fabrication process, in particular during the drying and calendaring step owing to a lower surface tension, a greater plasticity,

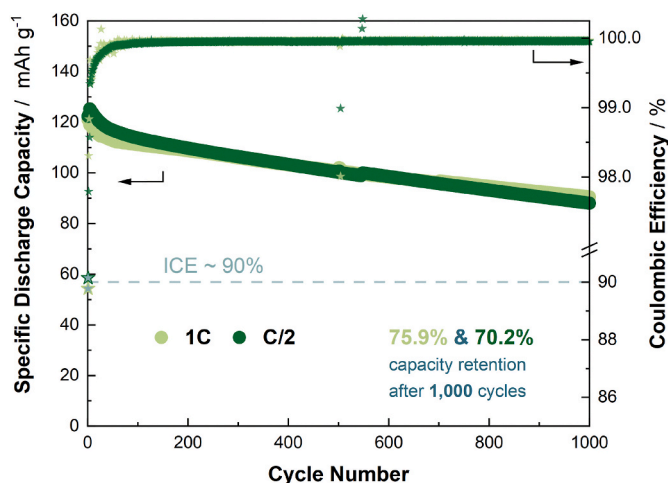


Fig. 8. Galvanostatic cycling of graphite||LNMO Li-ion cells at C/2 (in black) and 1C (in grey) with a CCCV charging protocol after three constant current formation cycles at C/5 (cut-off voltages: 2.8 and 4.9 V); the specific capacity refers to the active material mass loading of the CAR + CA-based LNMO cathode, which is about 20 mg cm^{-2} .

and the lower viscosity, enabling a higher solid content in the electrode slurry.

Finally, as a proof of concept, graphite||LNMO cells were assembled employing high mass loading LNMO electrodes with an areal capacity of about 2.5 mAh cm^{-2} . These lithium-ion cells had a high first cycle Coulombic efficiency of around 90% and reached an excellent initial capacity of 128 mAh g^{-1} at C/2 and 119 mAh g^{-1} at 1C (Fig. 8). These capacity values are comparable to the ones obtained in Li||LNMO cells, highlighting the great potential of CAR + CA as binder system for commercial-scale LNMO electrodes. In fact, the Coulombic efficiency remained above 99.9% during the subsequent cycling and the cells retained 75.9% and 70.2% of its capacity after 1000 cycles at 1C and C/2, respectively.

While the slightly inferior capacity retention at C/2 underlines the need to simultaneously enhance the interfacial stability at the LNMO|electrolyte interface, e.g., by optimizing the electrolyte composition and/or applying stabilizing surface coatings, the very good performance of these full-cells with industrially relevant mass loadings and areal capacities highlights the great promise of this novel, commercially available, fluorine-free binder system.

4. Conclusion

Water-soluble and fluorine-free carrageenan and, in particular, citric acid-crosslinked carrageenan is a very effective binder for $\text{LiNi}_{0.5}\text{Mn}_{1.5}\text{O}_4$ (LNMO) cathodes, enabling the fabrication of sufficiently flexible and mechanically stable electrodes with a commercially relevant active material mass loading of 20 mg cm^{-2} . These electrodes show good performance in half-cells and graphite||LNMO full-cells with an average Coulombic efficiency of 99.95% and a capacity retention of 75.9% after 1000 cycles at 1C. The advantageous properties of carrageenan originate from its greater reduction of the surface tension of water, its suitable plasticity, and its lower viscosity, allowing for a higher solid content of the corresponding electrode slurry. The comparison with PVdF-based LNMO electrodes reveals a comparable performance, underlining the great promise of this new and much more sustainable binder system. Given that these advantageous properties are intrinsic to (crosslinked) carrageenan, we may anticipate that it allows also for the realization of high mass loading electrodes employing other lithium and presumably also sodium cathode materials. Generally, the realization of well-performing high mass loading electrodes is an important step towards the commercialization of aqueous electrode

fabrication processes and may add to the realization of more sustainable and less costly rechargeable batteries in the near future.

CRediT authorship contribution statement

Markus Binder: Writing – original draft, Methodology, Investigation, Formal analysis, Data curation, Conceptualization. **Eva Keller:** Investigation, Formal analysis, Data curation. **Dominic Bresser:** Writing – review & editing, Supervision, Resources, Project administration, Methodology, Funding acquisition, Conceptualization.

Declaration of competing interest

The authors declare the following financial interests/personal relationships which may be considered as potential competing interests: Dominic Bresser reports financial support was provided by Federal Ministry of Education and Research Bonn Office. If there are other authors, they declare that they have no known competing financial interests or personal relationships that could have appeared to influence the work reported in this paper.

Data availability

Data will be made available on request.

Acknowledgement

The authors would like to acknowledge financial support from the German Federal Ministry of Education and Research (BMBF) within the ExcellBattUlm (03XP0257D) project and from the Helmholtz Association.

Appendix A. Supplementary data

Supplementary data to this article can be found online at <https://doi.org/10.1016/j.jpowsour.2024.234487>.

References

- [1] M. Wentker, M. Greenwood, J. Leker, A bottom-up approach to lithium-ion battery cost modeling with a focus on cathode active materials, *Energies* 12 (2019) 1–18, <https://doi.org/10.3390/en12030504>.
- [2] S. van den Brink, R. Kleijn, B. Sprecher, A. Tukker, Identifying supply risks by mapping the cobalt supply chain, *Resour. Conserv. Recycl.* 156 (2020) 104743, <https://doi.org/10.1016/j.resconrec.2020.104743>.
- [3] W. Li, B. Song, A. Manthiram, High-voltage positive electrode materials for lithium-ion batteries, *Chem. Soc. Rev.* 46 (2017) 3006–3059, <https://doi.org/10.1039/c6cs00875e>.
- [4] M. Armand, P. Axmann, D. Bresser, M. Copley, K. Edström, C. Ekberg, D. Guyomard, B. Lestriez, P. Novák, M. Petranikova, W. Porcher, S. Trabesinger, M. Wohlfahrt-Mehrens, H. Zhang, Lithium-ion batteries – current state of the art and anticipated developments, *J. Power Sources* 479 (2020) 228708, <https://doi.org/10.1016/j.jpowsour.2020.228708>.
- [5] Z. Jusys, M. Binder, J. Schnaidt, R.J.J. Behm, A novel DEMS approach for studying gas evolution at battery-type electrode|electrolyte interfaces: high-voltage $\text{LiNi}_{0.5}\text{Mn}_{1.5}\text{O}_4$ cathode in ethylene and dimethyl carbonate electrolytes, *Electrochim. Acta* 314 (2019) 188–201, <https://doi.org/10.1016/j.electacta.2019.05.076>.
- [6] B. Michalak, B.B. Berkes, H. Sommer, T. Brezesinski, J. Janek, Electrochemical cross-talk leading to gas evolution and capacity fade in $\text{LiNi}_{0.5}\text{Mn}_{1.5}\text{O}_4$ /graphite full-cells, *J. Phys. Chem. C* 121 (2017) 211–216, <https://doi.org/10.1021/acs.jpcc.6b11184>.
- [7] N.P.W. Pieczonka, Z. Liu, P. Lu, K.L. Olson, J. Moote, B.R. Powell, J.-H. Kim, Understanding transition-metal dissolution behavior in $\text{LiNi}_{0.5}\text{Mn}_{1.5}\text{O}_4$ high-voltage spinel for lithium ion batteries, *J. Phys. Chem. C* 117 (2013) 15947–15957, <https://doi.org/10.1021/jp405158m>.
- [8] M. Mancini, P. Axmann, G. Gabrielli, M. Kinyanjui, U. Kaiser, M. Wohlfahrt-Mehrens, A high-voltage and high-capacity $\text{Li}_{1+x}\text{Ni}_{0.5}\text{Mn}_{1.5}\text{O}_4$ cathode material: from synthesis to full lithium-ion cells, *ChemSusChem* 9 (2016) 1843–1849, <https://doi.org/10.1002/cssc.201600365>.
- [9] J.H. Kim, N.P.W. Pieczonka, Z. Li, Y. Wu, S. Harris, B.R. Powell, Understanding the capacity fading mechanism in $\text{LiNi}_{0.5}\text{Mn}_{1.5}\text{O}_4$ /graphite Li-ion batteries, *Electrochim. Acta* 90 (2013) 556–562, <https://doi.org/10.1016/j.electacta.2012.12.069>.

- [10] J. Song, D.W. Shin, Y. Lu, C.D. Amos, A. Manthiram, J.B. Goodenough, Role of oxygen vacancies on the performance of $\text{Li}[\text{Ni} 0.5\text{-xMn} 1.5\text{+ x}] \text{O}_4$ ($x = 0, 0.05, \text{ and } 0.08$) spinel cathodes for lithium-ion batteries, *Chem. Mater.* 24 (2012) 3101–3109, <https://doi.org/10.1021/cm301825h>.
- [11] J. Wang, W. Lin, B. Wu, J. Zhao, Syntheses and electrochemical properties of the Na-doped $\text{LiNi}_0.5\text{Mn}_1.5\text{O}_4$ cathode materials for lithium-ion batteries, *Electrochim. Acta* 145 (2014) 245–253, <https://doi.org/10.1016/j.electacta.2014.07.140>.
- [12] P. Stüble, H. Gebwein, S. Indris, M. Müller, J.R. Binder, On the electrochemical properties of the Fe-Ti doped LNMO material $\text{LiNi}_0.5\text{Mn}_1.37\text{Fe}_0.1\text{Ti}_0.03\text{O}_3.95$, *J. Mater. Chem. A* (2022) 9010–9024, <https://doi.org/10.1039/d2ta00299j>.
- [13] Y.Z. Jin, Y.Z. Lv, Y. Xue, J. Wu, X.G. Zhang, Z.B. Wang, Improved electrochemical performance of $\text{LiNi}_0.4\text{Ti}_0.1\text{Mn}_1.5\text{O}_4$ as cathode of lithium ion battery by carbon-coating, *RSC Adv.* 4 (2014) 57041–57047, <https://doi.org/10.1039/c4ra07921c>.
- [14] G. Gabrielli, P. Axmann, M. Wohlfahrt-Mehrens, Study of $\text{LiNi}_0.5\text{Mn}_1.5\text{O}_4$ morphological features for reduced electrolyte decomposition at high potential, *J. Electrochem. Soc.* 163 (2016) A470–A476, <https://doi.org/10.1149/2.0541603jes>.
- [15] M. Kuenzel, G.T. Kim, M. Zarrabetia, S.D. Lin, A.R. Schuer, D. Geiger, U. Kaiser, D. Bresser, S. Passerini, Crystal engineering of TMOx-coated $\text{LiNi}_0.5\text{Mn}_1.5\text{O}_4$ cathodes for high-performance lithium-ion batteries, *Mater. Today* 39 (2020) 127–136, <https://doi.org/10.1016/j.mattod.2020.04.003>.
- [16] K.R. Chemelewski, D.W. Shin, W. Li, A. Manthiram, Octahedral and truncated high-voltage spinel cathodes: the role of morphology and surface planes in electrochemical properties, *J. Mater. Chem. A* 1 (2013) 3347–3354, <https://doi.org/10.1039/c3ta00682d>.
- [17] J. Shi, Z. Wang, Y.Q. Fu, Density functional theory analysis of surface structures of spinel $\text{LiNi}_0.5\text{Mn}_1.5\text{O}_4$ cathode materials, *J. Mater. Sci.* 52 (2017) 605–612, <https://doi.org/10.1007/s10853-016-0357-y>.
- [18] A. Kazzazi, D. Bresser, M. Kuenzel, M. Hekmatfar, J. Schnaidt, Z. Jusys, T. Diemant, R.J. Behm, M. Copley, K. Maranski, J. Cookson, I. de Meazza, P. Axmann, M. Wohlfahrt-Mehrens, S. Passerini, Synergistic electrolyte additives for enhancing the performance of high-voltage lithium-ion cathodes in half-cells and full-cells, *J. Power Sources* 482 (2021) 228975, <https://doi.org/10.1016/j.jpowsour.2020.228975>.
- [19] A. Hofmann, A. Höweling, N. Bohn, M. Müller, J.R. Binder, T. Hanemann, Additives for cycle life improvement of high-voltage LNMO-based Li-ion cells, *ChemElectro Chem* 6 (2019) 5255–5263, <https://doi.org/10.1002/celec.201901120>.
- [20] N.P.W. Elise, R. Østli, Alma Mathew, Julian R. Tolchar, Daniel Brandell, Ann Mari Svensson, Sverre M. Selbach, Stabilizing the cathode interphase of LNMO using an ionic-liquid based electrolyte, *Batter. Supercaps.* (2023) 1–23, <https://doi.org/10.1002/batt.202300085>.
- [21] V. Tarnopolskiy, J. Kalhoff, M. Nádherná, D. Bresser, L. Picard, F. Fabre, M. Rey, S. Passerini, Beneficial influence of succinic anhydride as electrolyte additive on the self-discharge of 5 v $\text{LiNi}_0.4\text{Mn}_1.6\text{O}_4$ cathodes, *J. Power Sources* 236 (2013) 39–46, <https://doi.org/10.1016/j.jpowsour.2013.02.030>.
- [22] N.S. Choi, J.G. Han, S.Y. Ha, I. Park, C.K. Back, Recent advances in the electrolytes for interfacial stability of high-voltage cathodes in lithium-ion batteries, *RSC Adv.* 5 (2015) 2732–2748, <https://doi.org/10.1039/c4ra11575a>.
- [23] T. Fu, D. Lu, Z. Yao, Y. Li, C. Luo, T. Yang, S. Liu, Y. Chen, Q. Guo, C. Zheng, W. Sun, Advances in modification methods and the future prospects of high-voltage spinel $\text{LiNi}_0.5\text{Mn}_1.5\text{O}_4$ — a review, *J. Mater. Chem. A* 11 (2023) 13889–13915, <https://doi.org/10.1039/d3ta01777j>.
- [24] D. Di Lecce, R. Verrilli, J. Hassoun, Lithium-ion batteries for sustainable energy storage: recent advances towards new cell configurations, *Green Chem.* 19 (2017) 3442–3467, <https://doi.org/10.1039/c7gc01328k>.
- [25] J. Li, Y. Lu, T. Yang, D. Ge, D.L. Wood, Z. Li, Water-based electrode manufacturing and direct recycling of lithium-ion battery electrodes—a green and sustainable manufacturing system, *iScience* 23 (2020) 101081, <https://doi.org/10.1016/j.isci.2020.101081>.
- [26] R. Shunmugasundaram, R. Senthil Arumugam, P. Benedek, M. Yarema, P. Baade, V. Wood, In situ formation of lithium polyacrylate binder for aqueous manufacturing and recycling of Ni-rich cathodes, *J. Electrochem. Soc.* 169 (2022) 060504, <https://doi.org/10.1149/1945-7111/ac7171>.
- [27] D.E. Malek, L.A. Malley, T.W. Slone, G.S. Elliott, G.L. Kennedy, W. Mellert, K. Deckardt, C. Gemhardt, B. Hildebrand, S.R. Murphy, D.B. Bower, G.A. Wright, Repeated dose toxicity study (28 days) in rats and mice with N-methylpyrrolidone (NMP), *Drug Chem. Toxicol.* 20 (1997) 63–77, <https://doi.org/10.3109/01480549709011079>.
- [28] K.P. Lee, N.C. Chromey, R. Culik, J.R. Barnes, P.W. Schneider, Toxicity of N-methyl-2-pyrrolidone (NMP): teratogenic, subchronic, and two-year inhalation studies, *Toxicol. Sci.* 9 (1987) 222–235, <https://doi.org/10.1093/toxsci/9.2.222>.
- [29] S. Radloff, R.-G. Scurtu, M. Hölzle, M. Wohlfahrt-Mehrens, Applying established water-based binders to aqueous processing of $\text{LiNi}_0.83\text{Co}_0.12\text{Mn}_0.05\text{O}_2$ positive electrodes, *J. Electrochem. Soc.* 168 (2021) 100506, <https://doi.org/10.1149/1945-7111/ac2861>.
- [30] M. Kuenzel, D. Bresser, T. Diemant, D.V. Carvalho, G.T. Kim, R.J. Behm, S. Passerini, Complementary strategies toward the aqueous processing of high-voltage $\text{LiNi}_0.5\text{Mn}_1.5\text{O}_4$ lithium-ion cathodes, *ChemSusChem* 11 (2018) 562–573, <https://doi.org/10.1002/cssc.201702021>.
- [31] Z.W. Yin, T. Zhang, S.J. Zhang, Y.P. Deng, X.X. Peng, J.Q. Wang, J.T. Li, L. Huang, H. Zheng, S.G. Sun, Understanding the role of water-soluble guar gum binder in reducing capacity fading and voltage decay of Li-rich cathode for Li-ion batteries, *Electrochim. Acta* 351 (2020) 136401, <https://doi.org/10.1016/j.electacta.2020.136401>.
- [32] T. Zhang, J.T. Li, J. Liu, Y.P. Deng, Z.G. Wu, Z.W. Yin, D. Guo, L. Huang, S.G. Sun, Suppressing the voltage-fading of layered lithium-rich cathode materials via an aqueous binder for Li-ion batteries, *Chem. Commun.* 52 (2016) 4683–4686, <https://doi.org/10.1039/c5cc10534j>.
- [33] M. Kuenzel, H. Choi, F. Wu, A. Kazzazi, P. Axmann, M. Wohlfahrt-Mehrens, D. Bresser, S. Passerini, Co-crosslinked water-soluble biopolymers as a binder for high-voltage $\text{LiNi}_0.5\text{Mn}_1.5\text{O}_4$ /Graphite lithium-ion full cells, *ChemSusChem* 13 (2020) 2650–2660, <https://doi.org/10.1002/cssc.201903483>.
- [34] H. Gao, W. Zhou, J.H. Jang, J.B. Goodenough, Cross-linked chitosan as a polymer network binder for an antimony anode in sodium-ion batteries, *Adv. Energy Mater.* 6 (2016) 1–7, <https://doi.org/10.1002/aenm.201502130>.
- [35] M. Kuenzel, R. Porhiel, D. Bresser, J. Asenbauer, P. Axmann, M. Wohlfahrt-Mehrens, S. Passerini, Deriving structure-performance relations of chemically modified chitosan binders for sustainable high-voltage $\text{LiNi}_0.5\text{Mn}_1.5\text{O}_4$ cathodes, *Batter. Supercaps.* 3 (2020) 155–164, <https://doi.org/10.1002/batt.201900140>.
- [36] F. Bigoni, F. De Giorgio, F. Soavi, C. Arbizzani, Sodium alginate: a water-processable binder in high-voltage cathode formulations, *J. Electrochem. Soc.* 164 (2016) A6171–A6177, <https://doi.org/10.1149/2.0281701jes>.
- [37] M.H. Ryou, S. Hong, M. Winter, H. Lee, J.W. Choi, Improved cycle lives of LiMn_2O_4 cathodes in lithium ion batteries by an alginate biopolymer from seaweed, *J. Mater. Chem. A* 1 (2013) 15224–15229, <https://doi.org/10.1039/c3ta13514d>.
- [38] D. Bresser, D. Buchholz, A. Moretti, A. Varzi, S. Passerini, Alternative binders for sustainable electrochemical energy storage: the transition to aqueous electrode processing and bio-derived polymers, *Energy Environ. Sci.* 11 (2018) 3096–3127, <https://doi.org/10.1039/c8ee00640g>.
- [39] N. Loeffler, J. Von Zamory, N. Laszczynski, I. Doberdo, G.T. Kim, S. Passerini, Performance of $\text{LiNi}_1/3\text{Mn}_1/3\text{Co}_1/3\text{O}_2$ /graphite batteries based on aqueous binder, *J. Power Sources* 248 (2014) 915–922, <https://doi.org/10.1016/j.jpowsour.2013.10.018>.
- [40] T. Kazda, D. Capková, K. Jaššo, A.F. Straková, E. Shembel, A. Markevich, M. Sedlářiková, Carrageenan as an ecological alternative of polyvinylidene difluoride binder for li-s batteries, *Materials* 14 (2021) 1–11, <https://doi.org/10.3390/ma14195578>.
- [41] W. Jang, K.K. Rajeev, G.M. Thorat, S. Kim, Y. Kang, T.H. Kim, Lambda carrageenan as a water-soluble binder for silicon anodes in lithium-ion batteries, *ACS Sustain. Chem. Eng.* 10 (2022) 12620–12629, <https://doi.org/10.1021/acscuschemeng.2c03313>.
- [42] A.C. Rolandi, C. Pozo-Gonzalo, I. de Meazza, N. Casado, M. Forsyth, D. Mecerreyes, Carrageenans as sustainable water-processable binders for high-voltage NMC_{811} cathodes, *ACS Appl. Energy Mater.* 6 (2023) 8616–8625, <https://doi.org/10.1021/acsaem.3c01662>.
- [43] J. Necas, L. Bartosikova, Carrageenan: a review, *Vet. Med. (Praha)*. 58 (2013) 187–205, <https://doi.org/10.17221/6758-VETMED>.
- [44] L. Piculell, S. Nilsson, P. Muhrbeck, Effects of small amounts of kappa-carrageenan on the rheology of aqueous iota-carrageenan, *Carbohydr. Polym.* 18 (1992) 199–208, [https://doi.org/10.1016/0144-8617\(92\)90064-w](https://doi.org/10.1016/0144-8617(92)90064-w).
- [45] J. Doyle, P. Giannouli, K. Philip, E.R. Morris, Effect Ca^{2+} Cations on Gealton of K-Carrageenan, *Rheol. Asp.* (n.d.).
- [46] P. Stüble, M. Müller, T. Bergfeldt, J.R. Binder, A. Hofmann, Cycling stability of lithium-ion batteries based on Fe–Ti-doped $\text{LiNi}_0.5\text{Mn}_1.5\text{O}_4$ cathodes, graphite anodes, and the cathode-additive Li_3PO_4 , *Adv. Sci.* 10 (2023) 1–15, <https://doi.org/10.1002/adv.202301874>.
- [47] M. Hofmann, F. Nagler, M. Kapuschinski, U. Guntow, G.A. Giffin, Surface modification of $\text{LiNi}_0.8\text{Co}_0.15\text{Al}_0.05\text{O}_2$ particles via Li_3PO_4 coating to enable aqueous electrode processing, *ChemSusChem* 13 (2020) 5962–5971, <https://doi.org/10.1002/cssc.202001907>.
- [48] Z. Chen, G.T. Kim, D. Bresser, T. Diemant, J. Asenbauer, S. Jeong, M. Copley, R. J. Behm, J. Lin, Z. Shen, S. Passerini, MnPO_4 -Coated $\text{Li}(\text{Ni}_0.4\text{Co}_0.2\text{Mn}_0.4)\text{O}_2$ for lithium(-ion) batteries with outstanding cycling stability and enhanced lithiation kinetics, *Adv. Energy Mater.* 8 (2018) 1–13, <https://doi.org/10.1002/aenm.201801573>.
- [49] W. Haselrieder, B. Westphal, H. Bockholt, A. Diener, S. Höft, A. Kwade, Measuring the coating adhesion strength of electrodes for lithium-ion batteries, *Int. J. Adhesion Adhes.* 60 (2015) 1–8, <https://doi.org/10.1016/j.ijadhadh.2015.03.002>.
- [50] Y.W. Wardhana, N. Aanisah, I. Sopyan, R. Hendriani, A.Y. Chaerunisaa, Gelling power alteration on kappa-carrageenan dispersion through esterification method with different fatty acid saturation, *Gels* 8 (2022) 752, <https://doi.org/10.3390/gels8110752>.
- [51] D.L. Wood, J. Li, C. Daniel, Prospects for reducing the processing cost of lithium ion batteries, *J. Power Sources* 275 (2015) 234–242, <https://doi.org/10.1016/j.jpowsour.2014.11.019>.
- [52] J. Asenbauer, T. Eisenmann, M. Kuenzel, A. Kazzazi, Z. Chen, D. Bresser, The success story of graphite as a lithium-ion anode material—fundamentals, remaining challenges, and recent developments including silicon (oxide) composites, *Sustain. Energy Fuels* 4 (2020) 5387–5416, <https://doi.org/10.1039/d0se00175a>.
- [53] J.H. Kim, N.P.W. Pieczonka, L. Yang, Challenges and approaches for high-voltage spinel lithium-ion batteries, *ChemPhysChem* 15 (2014) 1940–1954, <https://doi.org/10.1002/cphc.201400052>.
- [54] G. Liang, V.K. Peterson, K.W. See, Z. Guo, W.K. Pang, Developing high-voltage spinel $\text{LiNi}_0.5\text{Mn}_1.5\text{O}_4$ cathodes for high-energy-density lithium-ion batteries: current achievements and future prospects, *J. Mater. Chem. A* 8 (2020) 15373–15398, <https://doi.org/10.1039/d0ta02812f>.
- [55] F. De Giorgio, N. Laszczynski, J. von Zamory, M. Mastragostino, C. Arbizzani, S. Passerini, Graphite/ $\text{LiNi}_0.5\text{Mn}_1.5\text{O}_4$ cells based on environmentally friendly

- made-in-water electrodes, *ChemSusChem* 10 (2017) 379–386, <https://doi.org/10.1002/cssc.201601249>.
- [56] M.T. Nguyen, H.Q. Pham, J.A. Berrocal, I. Gunkel, U. Steiner, An electrolyte additive for the improved high voltage performance of LiNi_{0.5}Mn_{1.5}O₄ (LNMO) cathodes in Li-ion batteries, *J. Mater. Chem. A* 11 (2023) 7670–7678, <https://doi.org/10.1039/d2ta09930f>.
- [57] N. Elgrishi, K.J. Rountree, B.D. McCarthy, E.S. Rountree, T.T. Eisenhart, J. L. Dempsey, A practical beginner's guide to cyclic voltammetry, *J. Chem. Educ.* 95 (2018) 197–206, <https://doi.org/10.1021/acs.jchemed.7b00361>.
- [58] N. Ogihara, S. Kawauchi, C. Okuda, Y. Itou, Y. Takeuchi, Y. Ukyo, Theoretical and experimental analysis of porous electrodes for lithium-ion batteries by electrochemical impedance spectroscopy using a symmetric cell, *J. Electrochem. Soc.* 159 (2012) A1034–A1039, <https://doi.org/10.1149/2.057207jes>.
- [59] T.T. Nguyen, A. Demortière, B. Fleutot, B. Delobel, C. Delacourt, S.J. Cooper, The electrode tortuosity factor: why the conventional tortuosity factor is not well suited for quantifying transport in porous Li-ion battery electrodes and what to use instead, *npj Comput. Mater.* 6 (2020), <https://doi.org/10.1038/s41524-020-00386-4>.
- [60] S. Baazouzi, N. Feistel, J. Wanner, I. Landwehr, A. Fill, K.P. Birke, Design, properties, and manufacturing of cylindrical Li-ion battery cells—a generic overview, *Batteries* 9 (2023), <https://doi.org/10.3390/batteries9060309>.
- [61] J. Li, J. Fleetwood, W.B. Hawley, W. Kays, From materials to cell: state-of-the-art and prospective technologies for lithium-ion battery electrode processing, *Chem. Rev.* 122 (2022) 903–956, <https://doi.org/10.1021/acs.chemrev.1c00565>.
- [62] B. Westphal, H. Bockholt, A. Kwade, Influence of convective drying parameters on electrode performance and physical electrode properties, *ECS Meet. Abstr.* MA2014-02 (2014) 328, <https://doi.org/10.1149/ma2014-02/5/328>, 328.
- [63] M. Müller, L. Pfaffmann, S. Jaiser, M. Baunach, V. Trouillet, F. Scheiba, P. Scharfer, W. Schabel, W. Bauer, Investigation of binder distribution in graphite anodes for lithium-ion batteries, *J. Power Sources* 340 (2017) 1–5, <https://doi.org/10.1016/j.jpowsour.2016.11.051>.
- [64] B.G. Westphal, A. Kwade, Critical electrode properties and drying conditions causing component segregation in graphitic anodes for lithium-ion batteries, *J. Energy Storage* 18 (2018) 509–517, <https://doi.org/10.1016/j.est.2018.06.009>.
- [65] C. Schilcher, C. Meyer, A. Kwade, Structural and electrochemical properties of calendered lithium manganese oxide cathodes, *Energy Technol.* 4 (2016) 1604–1610, <https://doi.org/10.1002/ente.201600130>.
- [66] S. Scheffler, R. Jagau, N. Müller, A. Diener, A. Kwade, Calendering of silicon-containing electrodes and their influence on the mechanical and electrochemical properties, *Batteries* 8 (2022) 46, <https://doi.org/10.3390/batteries8050046>.
- [67] N. Strzelczyk, L. Gottschalk, J. Müller, A. Kwade, The influence of calendering on the fast charging performance and lithium plating of hard carbon blend anodes, *Energy Technol.* (2022) 2200865, <https://doi.org/10.1002/ente.202200865>.
- [68] Z. Du, K.M. Rollag, J. Li, S.J. An, M. Wood, Y. Sheng, P.P. Mukherjee, C. Daniel, D. L. Wood, Enabling aqueous processing for crack-free thick electrodes, *J. Power Sources* 354 (2017) 200–206, <https://doi.org/10.1016/j.jpowsour.2017.04.030>.